1989

Oxygen Reduction in a Proton Exchange Membrane Test Cell

S. J. Ridge
Texas A & M University - College Station

Ralph E. White
University of South Carolina - Columbia, white@cec.sc.edu

Y. Tsou

R. N. Beaver

G. A. Eisman

Publication Info

Journal of the Electrochemical Society, 1989, pages 1902-1909.

DOI: 10.1149/1.2097078
http://dx.doi.org/10.1149/1.2097078

Oxygen Reduction in a Proton Exchange Membrane Test Cell

S. J. Ridge* and R. E. White**

Department of Chemical Engineering, Texas A&M University, College Station, Texas 77843-3122

Y. Tsou,** R. N. Beaver,** and G. A. Eisman**

Dow Chemical USA, Texas Applied Science and Technology Laboratories, Freeport, Texas 77541

ABSTRACT

Oxygen reduction in a gas-fed porous electrode attached to a proton exchange membrane is discussed. Experimental data and a mathematical model are presented for the test cell used. Various membrane and electrode assemblies were tested at different levels of platinum loading and Teflon®,[1] content. The model accounts for the diffusion and reaction of oxygen and the diffusion and reaction of hydrogen ions. Sulfuric acid was placed above the membrane in the test cell reservoir to provide a source of protons for the reduction of oxygen at the cathode. Based upon model predictions, it is shown that the transport of the protons in the active layer of the cathode is an important factor in the operation of the test cell.

The proton exchange membrane (PEM) fuel cell is of interest to developers of high power density electrical energy devices. Applications for PEM fuel cell technology are in the areas of space, electrical utilities, terrestrial vehicular power, and submarines for defense purposes (1). The aspects that make these fuel cells appealing are their small volume, light weight, high efficiency, and minimum noise. This fuel cell would be more useful if the losses due to the inefficient reduction of oxygen at the cathode (2) could be overcome. In order to do this, a better understanding of the mode of operation of the gas-fed oxygen reduction porous electrode is needed.

This understanding has been sought by others through the use of mathematical models. Two of these models that were used to characterize a gas diffusion porous electrode are the simple pore model by Austin (3) and the thin film model by Will (4). These are models that pertain only to the fundamental component of the electrode, such as a single pore or a thin film. Several models (5-8) have been developed recently that treat the electrode from a more macroscopic point of view. These models include physically measurable quantities other than just the pore radius. Most of these models have been applied to Teflon®-bonded electrodes either in phosphoric acid or alkaline electrolyte cells.

Most of these models are, however, limited in some way. The model presented by Giner and Hunter (5) includes the assumption that no ohmic losses occur in the electrode material and that there are no transport limitations in the gas phase. The model presented by Darby (6) and later extended by White *et al.* (7) includes the diffusion of both oxygen and hydrogen ions; however, they assumed that the potential in the electrode is constant and that only one model region exists, which is not true for a typical PEM fuel cell. The model presented by Iczkowski and Cutlip (8) is of the flooded agglomerate approach and includes two model regions: one for the porous backing layer and one for the active catalyst layer. Analogous to the thin film model by Will (4), the agglomerate is assumed to be covered by a thin film of electrolyte in which oxygen must first dissolve in the outer layer and then diffuse across the thin film before being consumed at the catalyst site inside the porous agglomerate. The Iczkowski and Cutlip model accounts for the diffusion of oxygen, nitrogen, and water in the gas-filled pores, electrochemical reaction of the oxygen dissolved in the agglomerate electrolyte, and electrical conduction. However, neither the Iczkowski and Cutlip model nor the Cutlip *et al.* (9) model include the diffusion and reaction of the hydrogen ions.

The mathematical model developed in this work is an attempt to explain the importance of the mechanism by which the reactants—oxygen and hydrogen ions—get to the catalyst site and react electrochemically. The model extends the Iczkowski and Cutlip model (8) by including the hydrogen ion concentration in the reaction rate expression and the transport equations associated with the hydrogen ion. These two extensions are coupled with the equations that describe the multicomponent gas-phase diffusion and solution potential in the active layer as recommended by Ross (10).

Experimental

Description of the test cell.—A schematic of the test cell and associated equipment is shown in Fig. 1. A PAR 175 universal programmer was used to sweep the potential at various scan rates. The output signal from the PAR 175 was fed into a PAR 173 potentiostat/galvanostat which was used to measure the current and potential of the porous electrode *vs.* a saturated calomel electrode (SCE) reference electrode. A Houston Instruments Model 2000 X-Y recorder was used to graph the potential *vs.* current output signals from the potentiostat/galvanostat.

The clear plastic half cell shown in Fig. 2 was used to obtain the electrochemical measurements on the gas-fed porous cathode. The membrane and electrode (M&E) assembly, with the electrode facing down, was placed between the two top pieces of the test cell which were then clamped together with bolts. The top piece of the half cell was used as a sulfuric acid reservoir to provide a source of protons to be transported through the membrane and consumed in the porous electrode. The bottom piece of the test cell was used to supply reactant gas to the porous electrode. This gas consisted typically of humidified oxygen which entered through the gas inlet port and flowed through the hollow cavity in the bottom piece of the cell and out of the cell through the gas outlet.

The M&E assembly was fabricated in a proprietary manner. It can be described, however, as consisting of the membrane and two layers: a porous backing layer made of carbon fiber paper and an active layer that was made of a

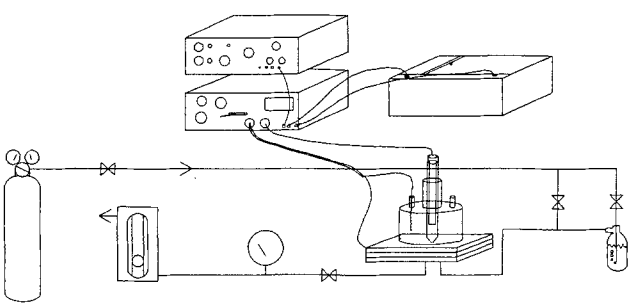

Fig. 1. Instrumentation and flow diagram

*Electrochemical Society Student Member.
**Electrochemical Society Active Member.
[1]Registered trademark of E. I. du Pont de Nemours and Company.

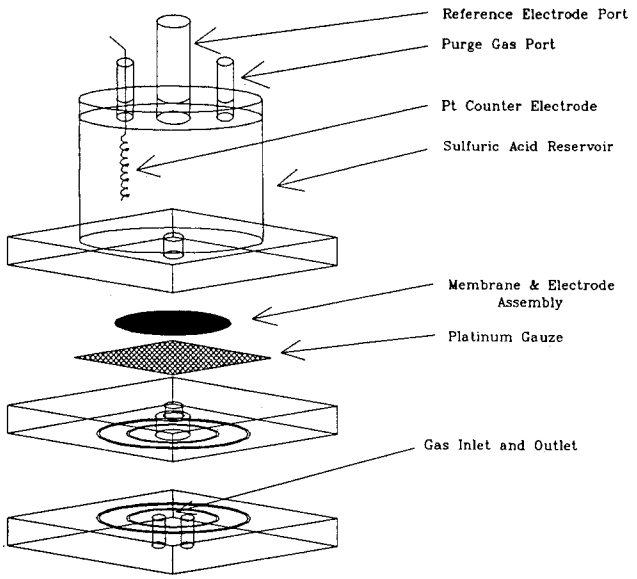

Fig. 2. Test cell schematic

mixture of platinum particles and tetrafluoroethylene (Teflon®, TFE) binder. Dow membrane was used in each M&E sample.

Platinum gauze was placed underneath the porous electrode (working electrode) of the M&E to serve as a current collector. The counterelectrode was a platinum wire placed in the sulfuric acid reservoir and a removable Pyrex Luggin was set into place through the center hole in the top of the acid compartment. The tip of the Luggin was placed in the hole drilled through the bottom of the acid compartment (see Fig. 2) so that the Luggin tip was in firm contact with the membrane of the M&E being tested; this placement of the Luggin tip was used because it provided reproducible results. A saturated calomel electrode (SCE) was used to measure the potential at the membrane/acid interface.

Purified oxygen from a cylinder was fed either directly to the test cell or to a humidifier where the gas was bubbled through a container partially filled with water. The gas pressure in the test cell was monitored using a pressure gauge located on the stainless steel tubing downstream of the test cell. A rotameter was used to measure the gas flow rate that was regulated by a valve downstream from the pressure gauge.

Experimental procedure.—The procedure used to test the porous electrode consisted of measuring potentiostatically the polarization curve for the M&E by sweeping the potential from 1.2V (*vs.* SHE) to lower potentials. A scan rate of 5 mV/s was used to sweep the potential. Humidified oxygen at 24.7 psia and room temperature was fed to the porous electrode compartment of the cell at approximately 30 cm^3/min.

Experimental Results

The oxygen flow rate, oxygen pressure, and acid concentration were varied to determine qualitatively their influence on the experimental measurements. The effect of varying the oxygen flow rate over the range of the rotameter from 10 to 400 cm^3/min showed no significant change in the measured polarization curve over the range from 0 to 1500 mA/cm^2. Varying the oxygen pressure over the range of 16.7-34.7 psia caused a slight shift in the polarization curve toward higher potentials at higher pressures as would be expected.

The effect of varying the acid concentration was determined by measuring the polarization curve for three different acid strengths (0.92, 0.58, and 0.21*M*). This was done by keeping the M&E sample in the test cell and using three different acid strengths. The acid compartment of the test cell was thoroughly rinsed with deionized water after each test. The polarization curve for the 0.92*M* acid showed better performance compared to the other two acid strengths.

Table I. Current *vs.* potential (*vs.* SHE) varying [H_2SO_4]

[H_2SO_4] (*M*)	100 mA/cm^2 (V)	500 mA/cm^2 (V)	1000 mA/cm^2 (V)
0.21	0.78	0.72	0.67
0.58	0.79	0.75	0.71
0.92	0.82	0.77	0.74

For example, at a measured current density of 1000 mA/cm^2 the potential using 0.92*M* H_2SO_4 was 7 mV higher than that using 0.21*M* H_2SO_4. The performance results are summarized in Table I. All of the potentials in the table were read from measured polarization curves obtained by sweeping the potential at a scan rate of 5 mV/s and are relative to the SHE. The reversible potential for this process is 1.229V so that high potentials indicate better performance. The potentials presented have not been corrected for IR drop because the IR drop through the membrane was low due to the presence of the sulfuric acid in the membrane. Also, IR drops measured by using the current interrupt method were found to be very low.

The fact that the polarization curves were different for the same sample when the sulfuric acid concentration was varied is consistent with previous observations for Nafion®,[2] membranes (11-13). To confirm further that some H_2SO_4 is able to penetrate the membrane and thus the porous electrode structure, a $BaCl_2$ solution was applied to the active layer surface of the electrode before it was pressed onto the membrane. Since the barium from $BaCl_2$ precipitates as $BaSO_4$ in the presence of SO_4^{2-}, a white precipitate would indicate that H_2SO_4 was present in the active layer of the porous electrode. This test resulted in a white precipitate visible beneath the membrane surface between the membrane and the porous electrode. The precipitate that formed was the same size as the test cell hole in which the acid contacted the M&E. The only other source of sulfate ions would be from the membrane polymer side chains; however, if the side chains reacted with the $BaCl_2$, the whole surface between the membrane and electrode would have turned white. This was not the case. The significance of this test is discussed later.

In addition to varying some of the experimental conditions, certain active layer fabrication parameters were varied also. This was done while keeping the porous layer fabrication parameters and experimental conditions constant. The experimental conditions kept constant were temperature at 25°C, oxygen pressure at 10 psig, oxygen flow rate at 30 cm^3/min, relative humidity at 85%, and acid concentration at 0.92*M*, Dow membrane, the porous backing layer held at 10% (weight) TFE in the carbon fiber paper, and 2 mg/cm^2 platinum in the active layer.

The effect of varying the percent Teflon® (TFE) in the active layer was investigated using 5, 10, 15, 25, and 35% TFE samples while holding the other fabrication parameters constant, as mentioned above. These results are compared in Fig. 3 at five different current densities. The 10% TFE samples showed the best performance over the current density range from 100 to 4000 mA/cm^2. It should be noted that this is not a major effect, however. For example, at 100 mA/cm^2 the potential of the 10% TFE sample is only 18 mV higher than the potential of the 15% TFE sample and at higher current densities, the better performance is even less pronounced.

The effect of varying the platinum loading in the active layer was investigated with the same fabrication and operating parameters mentioned above except that the percent TFE in the active layer was kept constant at 10% TFE while the platinum loading was varied using 4, 2, and 1 mg/cm^2 Pt. The polarization curves measured using these three samples were nearly identical, as shown in Table II. For example, at 2000 mA/cm^2 current density, the potential of the 2 mg/cm^2 Pt sample is identical to that of the 1 mg/cm^2 Pt sample and only 7 mV lower than the potential of the 4 mg/cm^2 Pt sample. The platinum particles used in these samples were vendor 1 platinum.

[2]Registered trademark of E. I. du Pont de Nemours and Company.

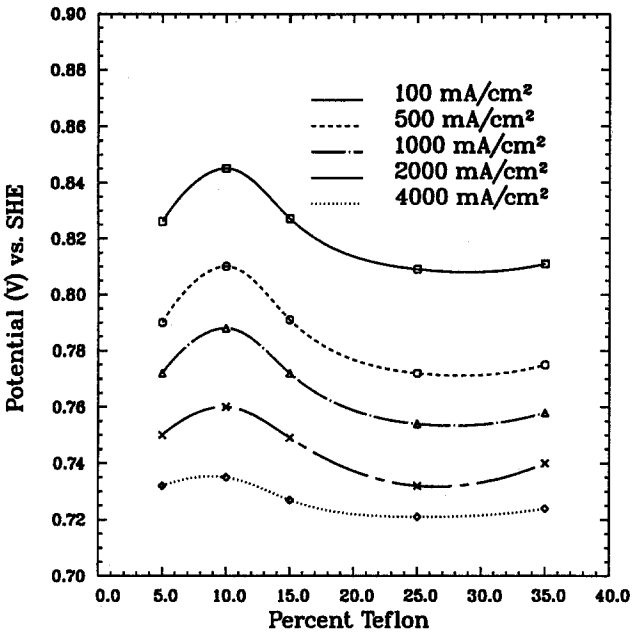

Fig. 3 Effect of Teflon® on performance

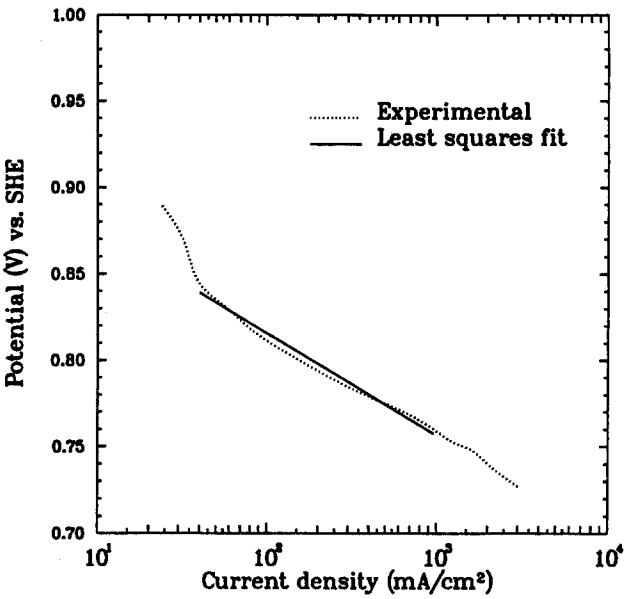

Fig. 4. Least squares fit of 15% TFE data for determining the Tafel slope.

When different sized platinum particles were used, there was a noticeable difference in performance. The electrode made with the smaller platinum particles (4 mg/cm^2) performed better. These results are shown in Table III. At 500 mA/cm^2 current density, the 4 mg/cm^2 Pt sample was 36 mV higher than the 2 mg/cm^2 Pt sample.

Analysis of Results

It appears from the experimental results that varying the acid concentration and the $BaSO_4$ precipitate in the porous electrode, that the sulfuric acid penetrates through the ion exchange membrane and into the porous electrode. This means that the test cell results presented here are different from what would be expected in a typical electrolyte-free PEM fuel cell. This is true because the sulfuric acid in the PEM provides a better means for transferring protons out of the membrane to the catalyst surface. The sulfuric acid can then be thought of as a molecular bridge (similar to the ionomer side chain structure only with a much lower equivalent weight) in which protons are more easily transported from the membrane/active layer interface via sulfonate side chains.

The results obtained by varying the Teflon® content (Fig. 3) indicate that the optimum percent Teflon® in the active layer is 10%. The performance of the 5% TFE sample was probably lower due to the lower hydrophobicity associated with the lower Teflon® content. That is, a Teflon® content below 10% TFE has the effect of retaining more electrolyte in the active layer, thereby making the transport of dissolved oxygen to the catalyst surface more difficult. To increase the hydrophobicity, more Teflon® can be added, but this causes the electrode resistance to increase. This behavior is shown by the decrease in performance with the 15 and 25% TFE samples. Above 25% TFE, there appears to be a leveling-off effect as shown by comparing the 35 and 25% TFE samples.

For each of the five samples with different amounts of Teflon® in the active layer, the Tafel slope was determined from the slope of the approximately linear portion of the logarithm of the current density *vs.* potential graph. An example of this graph for the 15% TFE sample is shown in Fig. 4. The range of current density used to calculate the slope of the linear Tafel region was between 40 and 960 mA/cm^2. A least squares fit of the data over this range gave a Tafel slope of 59.6 mV and a correlation coefficient of 0.994. The same current density range, from 40 to 960 mA/cm^2, was used to calculate the Tafel slope for the other four samples and summarized in Table IV along with the respective correlation coefficients. These results indicate that the number of electrons involved in the rate-determining step is two.

Since the results using vendor 1 Pt showed little difference in performance when the Pt loading was varied from 4, 2, and 1 mg/cm^2, it would appear that only a fraction of the total platinum actually supports the electrochemical reaction. However, there was a difference in performance between the 4 and 2 mg/cm^2 Pt samples using vendor 2 platinum, indicating better utilization of platinum over a lower current density range. The difference between the two types of platinum is probably due to the different particle sizes. This concept is discussed further below in the discussion section.

Table II. Current *vs.* potential (*vs.* SHE) varying vendor 1 Pt loading

Pt (mg/cm^2)	100 mA/cm^2 (V)	500 mA/cm^2 (V)	1000 mA/cm^2 (V)	2000 mA/cm^2 (V)	4000 mA/cm^2 (V)
4	0.819	0.785	0.765	0.741	0.721
2	0.821	0.785	0.762	0.734	0.711
1	0.819	0.779	0.757	0.734	0.712

Table III. Current *vs.* potential (*vs.* SHE) varying vendor 2 Pt loading

Pt (mg/cm^2)	100 mA/cm^2 (V)	500 mA/cm^2 (V)	1000 mA/cm^2 (V)	2000 mA/cm^2 (V)	4000 mA/cm^2 (V)
4	0.845	0.773	—	—	—
2	0.809	0.737	0.706	—	—

Model Development

A mathematical model was developed to provide a means for predicting the performance of the oxygen reduction porous electrode and to gain a better understanding of the operating mechanisms of the electrode. The mathematical model presented by Iczkowski and Cutlip (8) was modified to do this. The new model accounts for the diffusion and reaction of oxygen and the diffusion and

Table IV. Tafel slopes (T_s) from experimental data

% TFE	T_s (mV)	Correlation coefficient
5	59.75	0.994
10	53.28	0.997
15	59.63	0.994
25	58.72	0.996
35	59.00	0.994
average value	58.08	

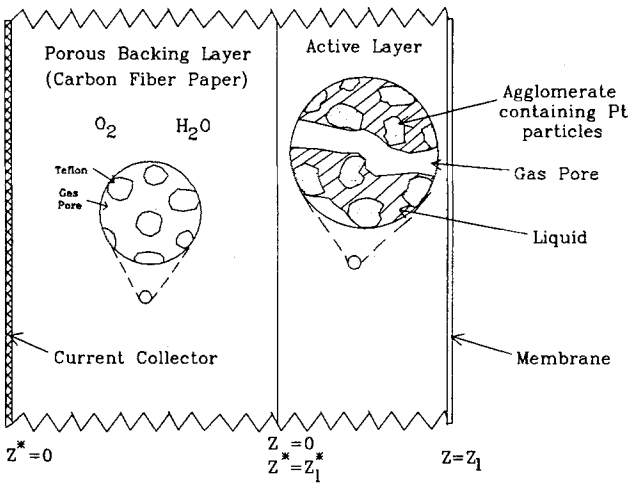

Fig. 5. Gas-fed porous electrode schematic

reaction of hydrogen ions. A schematic of the region included in the model is shown in Fig. 5.

Gas phase diffusion.—Humidified oxygen was used in the experiments for testing the porous electrode. Oxygen first diffuses through the porous backing layer, then diffuses and reacts in the active layer. The Stefan-Maxwell equation is used to describe the multicomponent diffusion in the two porous layers (14)

$$\nabla X_i = \sum_{j=1}^{m} \frac{(X_i N_j - X_j N_i)}{C D_{ij}^{eff}} \quad [1]$$

where m is set equal to two when considering the diffusion of oxygen and water. The mole fraction of each species, X_i, and the total molar concentration, C, can be written in terms of the component partial pressures and the total pressure by assuming ideal gas behavior

$$X_i = P_i/P_T \quad [2]$$

$$C = n/v = P_T/RT \quad [3]$$

The effective diffusion coefficient can be written in terms of the physical properties of the porous electrode (porosity and tortuosity) and the free stream binary diffusion coefficient

$$D_{ij}^{eff} = E_P D_{ij}^{\circ} \quad [4]$$

where E_P is the porosity divided by the tortuosity for the porous layer region.

In order to simplify the model equations, it is assumed that diffusion occurs only in one direction (Z and Z^*). Substituting Eq. [2]-[4] into Eq. [1] for $m = 2$ gives the oxygen and water diffusion equations in terms of partial pressures of each component

$$\frac{dP_{O_2}}{dZ^*} = \frac{RT}{E_P P_T D^{\circ}_{O_2,H_2O}} (P_{O_2} N_{H_2O} - P_{H_2O} N_{O_2}) \quad [5]$$

$$\frac{dP_{H_2O}}{dZ^*} = \frac{RT}{E_P P_T D^{\circ}_{O_2,H_2O}} (P_{H_2O} N_{O_2} - P_{O_2} N_{H_2O}) \quad [6]$$

Since the operating temperature of the cell during the experiments was room temperature, the water produced by the electrochemical reaction is liquid

$$O_2(g) + 4H^+(aq) + 4e \rightarrow 2H_2O(1) \quad [7]$$

It is assumed that water vapor carried in with the humidified oxygen also leaves the porous electrode as vapor; that is, there is no condensation or evaporation. The flux of water in the gas phase, N_{H_2O}, is then set equal to zero and Eq. [5] reduces to

$$\frac{dP_{O_2}}{dZ^*} = \frac{RT N_{O_2}}{E_P P_T D^{\circ}_{O_2,H_2O}} (P_{O_2} - P_T) \quad [8]$$

This assumption is used here for simplicity and is reasonable only for short-term experiments. For long-term experiments or steady-state conditions Eq. [5] and [6] would have to be solved simultaneously. This is different from the Iczkowski and Cutlip model (8) for a phosphoric acid fuel cell which operates at higher temperatures where it is assumed by them that all the water produced is in the vapor phase, counter diffusing with the oxygen.

After diffusing through the porous backing layer (see Fig. 5), the gas diffuses into the active layer. This process is also described by the Stefan-Maxwell equation by replacing E_P in Eq. [8] with E_T, the porosity/tortuosity factor in the active layer

$$\frac{dP_{O_2}}{dZ^*} = \frac{RT NO_2}{E_T P_T D^{\circ}_{O_2,H_2O}} (P_{O_2} - P_T) \quad [9]$$

In both the porous backing and active layers, it is assumed that the diffusion of the gases is entirely molecular diffusion and that any Knudsen diffusion is contained in the effective diffusion coefficient (15).

Agglomerate phase.—In the flooded agglomerate approach, the larger pores in the active layer provide gas diffusion paths, while the smaller micropores that make up the agglomerate are partially wetted by the electrolyte. Agglomerates consist of parallel porous cylinders of catalyst particles surrounded by electrolyte. The physical parameters that describe the agglomerate are E_n, the fraction of the electrode consisting of agglomerates; E_a, the porosity/tortuosity factor for the agglomerate; and r_a, the radius of the agglomerate.

Once the oxygen diffuses through the porous layer, it dissolves into the flooded agglomerate pores and is reduced electrochemically at the catalyst sites according to reaction [7]. The H^+ in reaction [7] is provided by protons from the sulfonate side chains of the membrane and from the sulfuric acid that penetrates through the membrane and into the active layer. The governing equations for the ionic species, H^+ and HSO_4^-, are derived from dilute solution theory (16). The material balance equation for the ionic species at steady state is given by

$$-\nabla \cdot N_i + R'_i = 0 \quad [10]$$

where R'_i is the production rate of species i due to electrochemical reaction within the porous agglomerate. Since four moles of protons are consumed for each mole of oxygen consumed, the reaction rate of H^+ is given by

$$R'_{H^+} = 4R'_{O_2} \quad [11]$$

where R'_{O_2} is the reaction rate of oxygen which is discussed in more detail below. The HSO_4^- ion does not react; therefore $R'_{HSO_4^-} = 0$.

The flux of liquid water produced by the electrochemical reaction [7] is twice the flux of the oxygen and in the opposite direction

$$N_{H_2O(1)} = -2N_{O_2} \quad [12]$$

The flux of ionic species i in the solution is due to migration in an electric field and diffusion in a concentration gradient

$$N_i = -z_i u_i \mathbf{F} C_i \nabla \Phi - D_i \nabla C_i \quad [13]$$

The ionic mobility, u_i, is described by the Nernst-Einstein equation

$$u_i = \frac{D_i}{RT} \quad [14]$$

Combining Eq. [10], [13], and [14], the one-dimensional governing equation for the ionic species in the agglomerate is

$$\frac{z_i D_i \mathbf{F}}{RT}\left(C_i \frac{d^2\Phi}{dZ^2} + \frac{dC_i}{dZ}\frac{d\Phi}{dZ}\right) + D_i \frac{d^2 C_i}{dZ^2} + R'_i = 0 \quad [15]$$

where the unknown quantities are Φ, the solution potential, and C_i, the concentration of each ionic species (H^+ and

HSO_4^-). The additional equation needed to complete the system of equations is given by the electroneutrality condition to ensure that there is no separation of charge

$$\sum_i z_i C_i = 0 \quad [16]$$

The potential, V, in the solid (catalyst) phase is described by Ohm's law

$$\frac{dV}{dz} = \frac{I_e(Z)}{\sigma_c} \quad [17]$$

where σ_c is the effective electronic conductivity and I_e is the electronic current density. The electronic current density produced by the consumption of oxygen is given by

$$I_e(Z) = -4\mathbf{F}N_{O_2}(Z) \quad [18]$$

where N_{O_2} is the flux of oxygen and is in the opposite direction of the electronic current density.

Reaction rate expression.—The flux of oxygen in the active layer varies with position since oxygen reacts electrochemically as it diffuses through the active layer. The governing equation for this process is given by the material balance equation for oxygen

$$\frac{dN_{O_2}(Z)}{dZ} = -R'_{O_2} \quad [19]$$

where R'_{O_2} is the local reaction rate of oxygen. In the film agglomerate model, the oxygen must diffuse across a thin film of electrolyte that covers the cylindrical agglomerate before the oxygen reacts in the pores of the agglomerate. Assuming the film is thin in comparison to the radius of the agglomerate and that the oxygen dissolved in the electrolyte at the gas pore/liquid interface is in equilibrium with the oxygen in the gas pore at that point, the reaction rate of oxygen in the agglomerate can be approximated by

$$R'_{O_2} = aD_{O_2}\frac{P_{O_2}(Z)C^o_{O_2} - C_{O_2}(r_a, Z)}{\delta} \quad [20]$$

where $P_{O_2}(Z)C^o_{O_2}$ is the concentration of dissolved oxygen at the surface of the electrolyte film; $C_{O_2}(r_a, Z)$ is the concentration of oxygen at the film/agglomerate interface; r_a is the agglomerate radius, Z is the position in the active layer; δ is the thickness of the film; a is the area of the film per unit volume of the electrode, and D_{O_2} is the diffusion coefficient of oxygen in the electrolyte.

The reaction rate term, R'_{O_2}, given by Iczkowski and Cutlip (8) is

$$R'_{O_2} = \epsilon_c K_e C_{O_2}(r_a, Z) \quad [21]$$

where the reaction is first order in the dissolved oxygen concentration with rate constant K_e and effectiveness factor ϵ_c. The rate constant, K_e, is written in terms of the activation current density, I_{act}, for which it is assumed that the reaction rate is limited by kinetics; that is, there is no rate limitation due to transport of reactants, thus

$$K_e = \frac{I_{act}}{4\mathbf{F}Z_l P^o_{O_2} C^o_{O_2}} \quad [22]$$

Iczkowski and Cutlip (8) applied Eq. [21] and [22] to a phosphoric acid fuel cell system in which the agglomerate is filled with acid electrolyte. This system is applicable to the porous electrodes tested in this study since it was previously determined that the sulfuric acid from the test cell reservoir penetrated through the membrane and into the electrode structure. However, Iczkowski and Cutlip (8) neglected to include the hydrogen ion concentration in the reaction rate equation. Damjanovic *et al.* (17) showed the reaction rate of oxygen to be first-order with respect to H^+ so that the reaction rate is given by

$$R'_{O_2} = \epsilon_c K'_e C_{H^+}(Z) C_{O_2}(r_a, Z) \quad [23]$$

where K_e is divided by a reference hydrogen ion concentration

$$K'_e = \frac{K_e}{C_{H^+,ref}} = \frac{I_{act}}{4\mathbf{F}Z_l P^o_{O_2} C^o_{O_2} C_{H^+,ref}} \quad [24]$$

By choosing a reference potential and corresponding current density from the data in the low current density activation region, the activation current density can be written as a function of potential in the Tafel form

$$I_{act} = I_{Er} \exp\left[\frac{2.303(E_r - E)}{T_s}\right] \quad [25]$$

where E_r and I_{Er} represent the reference potential and corresponding reference current density, respectively, and T_s, the Tafel slope. The electrochemical driving force, E, is defined as the difference between the electrode potential, V, and the electrolyte potential, Φ. The effectiveness factor for the cylindrical agglomerate is approximated by (18)

$$\epsilon_c = \frac{1}{M_c}\frac{3M_c \coth(3M_c) - 1}{3M_c} \quad [26]$$

where M_c is analogous to the Thiele modulus for porous catalyst

$$M_c = \frac{r_a}{2}\left[\frac{K'_e}{E_n E_a D}\right]^{1/2} \quad [27]$$

in which E_a is the porosity-tortuosity factor for the agglomerate, and E_n is the volume fraction of the electrode consisting of agglomerates.

The two expressions for R'_{O_2}, Eq. [20] and [23], can be combined to eliminate the dissolved oxygen at the surface of the agglomerate, $C_{O_2}(r_a, Z)$. The resulting equation for R'_{O_2} is in terms of the diffusion in the film and diffusion and reaction in the agglomerate

$$R'_{O_2} = \frac{P_{O_2}(Z)}{\frac{\delta}{aDC^o_{O_2}} + \frac{1}{\epsilon_c K'_e C^o_{O_2} C_{H^+}}} \quad [28]$$

Substituting Eq. [28] into [19] yields the differential equation for the flux of oxygen through the active layer

$$\frac{dN_{O_2}}{dZ} = \frac{-P_{O_2}(Z)}{\frac{\delta}{aDC^o_{O_2}} + \frac{1}{\epsilon_c K'_e C^o_{O_2} C_{H^+}}} \quad [29]$$

The formation of a thin film around the agglomerate is hindered from forming in the presence of an antiwetting agent such as Teflon® and is assumed here to be nonexistent. In terms of the model parameters, this means that δ is zero. This removes the diffusion resistance of the thin film so that oxygen dissolves directly into the micropores of the agglomerate. Equation [29] then reduces to

$$\frac{dN_{O_2}}{dZ} = -\epsilon_c K'_e C^o_{O_2} C_{H^+} P_{O_2}(Z) \quad [30]$$

This is referred to as the "dry agglomerate approach" (19) and is most likely to occur in the porous electrodes in this study since the antiwetting agent Teflon® was present in the active layer.

Boundary conditions.—The boundary conditions that apply to the gas/porous backing layer interface at $Z^* = 0$ are that the partial pressures of water and oxygen are given by the humidity and total pressure

$$P_{H_2O} = h_r P^*_{H_2O}/100\% \quad [31]$$

$$P_{O_2} = P_T - P_{H_2O} \quad [32]$$

These boundary conditions seem reasonable since the relative humidity of the inlet and outlet gas streams were measured and found to be essentially the same. This means that the amount of water added to the gas stream from the electrode was small relative to the amount of water in the gas supply stream. It would be useful to measure the amount of water added to the gas stream from the electrode and to change the boundary condition accordingly, but this was beyond the scope of this work. At the porous backing/active layer interface, the boundary condition for the gas phase is the continuity of partial pressures

$$P_{O_2}(Z = 0) = P_{O_2}(Z^* = Z_l^*) \quad [33]$$

$$P_{H_2O}(Z = 0) = P_{H_2O}(Z^* = Z_l^*) \quad [34]$$

For the agglomerate phase, the boundary condition at $Z = 0$ is zero flux for the ionic species (H^+ and HSO_4^-)

$$N_i(Z = 0) = 0 \quad [35]$$

The solution potential, Φ, is chosen to be zero at $Z = 0$, and the derivative of Φ is also zero at $Z = 0$

$$\Phi(Z = 0) = 0 \quad [36]$$

$$\frac{d\Phi}{dZ}(Z = 0) = 0 \quad [37]$$

The three remaining boundary conditions given at the active layer/membrane interface are the flux of oxygen is equal to zero; the potential difference between the electrode and electrolyte is equal to the reference potential; and the concentration of the ionic species is given

$$N_{O_2}(Z = Z_l) = 0 \quad [38]$$

$$V(Z = Z_l) - \Phi(Z = Z_l) = E_{ref} \quad [39]$$

$$C_i(Z = Z_l) = C_{ref} \quad [40]$$

In this case, the reference concentration is assumed to be that of the 0.92*M* H_2SO_4 in the test cell acid reservoir which penetrates through the membrane and into the porous electrode; however, the value used for C_{ref} is not critical for the predictions presented here. A value of 0.3*M* for C_{ref} would yield the same predicted current densities given below. This is true because the value for C_{ref} is important for limiting current conditions only which are never approached in this work.

Solution of the equations.—Equation [8] applies to the porous backing region, and Eq. [9], [15]-[17], and [30] are the six equations that apply to the active layer (Eq. [15] is used twice: once for $i = H^+$ and once for $i = HSO_4^-$).

Equation [8] is solved by applying the initial condition given in Eq. [32] and integrating through the thickness of the porous backing. The governing equations in the active layer are solved using a "shooting and correcting" method where the initial conditions given by Eq. [33], [35]-[37] are known and guesses are made for the initial values (at $Z = 0$) for N_{O_2}, V, and C_i. The governing equations are solved using a fourth order Runge-Kutta routine ("shooting") (20). Then the boundary values at $Z = Z_l$ for N_{O_2}, V, and C_i are compared with those given by Eq. [38]-[40]. When necessary, the initial guesses are corrected, and the governing equations are solved again until the solution boundary values agree with the given boundary conditions.

A Newton-Raphson algorithm is used for the convergence of the boundary values. Due to the complexity of the model equations, the derivative terms in the Newton-Raphson technique are determined numerically by perturbating one of the convergence variables (N_{O_2}, V, or C_i) while holding the others constant and solving the governing equations for that perturbation. This is equivalent to evaluating the partial derivatives numerically.

Discussion

Before discussing the results presented here, it is important to reiterate that the test gas-fed porous electrode used here was subject to permeation by approximately one molar sulfuric acid and, consequently, may not be representive of membrane electrodes with low conductivity water in the pore structure.

Tables II and III show that the size of the platinum particles affected the performance of the gas-fed porous electrodes used in this work. It is possible that the bigger particle size caused the agglomerate pores to become larger and consequently more wettable. This may have resulted in a larger effective, active catalyst area which gave better performance at low current density. However, at high current densities, the large amount of water produced caused a flooding problem and worse performance. This effect can be seen by comparing the performance of the electrodes made by using vendor 2 platinum particles to those made by using vendor 1 platinum particles (see Tables II and III) because the vendor 2 particles were bigger. An example comparing the model predictions with experimental data for the 10% TFE sample is shown in Fig. 6. These predictions were made by adjusting manually the model parameters (such as the agglomerate radius) until the model predictions matched closely the experimental data. The model parameters used to generate the polarization curve for this example are shown in Table V. The model predictions agree better with the data at high current densities where mass-transfer effects dominate. Unfortunately, at low current densities, the predicted potentials are too high.

The sensitivity of the porous electrode performance was tested as a function of some of the variable model parameters over a certain range and observing their effect on the predicted polarization curves. The variable parameters were grouped into a set of four unknown parameters similar to those used by White *et al.* (21)

$$\theta_1 = E_P$$

$$\theta_2 = E_T$$

$$\theta_3 = \frac{1}{\sigma_c}$$

$$\theta_4 = r_a/(E_n E_a)^{1/2}$$

The porosity of gas-fed electrodes is usually in the range of 20-70%, and the tortuosity is in the range of about $\sqrt{2}$-4 (2). Therefore, reasonable ranges for both E_P and E_T would be 0.50-0.05. The porous backing layer porosity/tortuosity factor, E_P, was varied over a wider range of 0.50-0.005 as was the active layer porosity/tortuosity factor, E_T. Both vari-

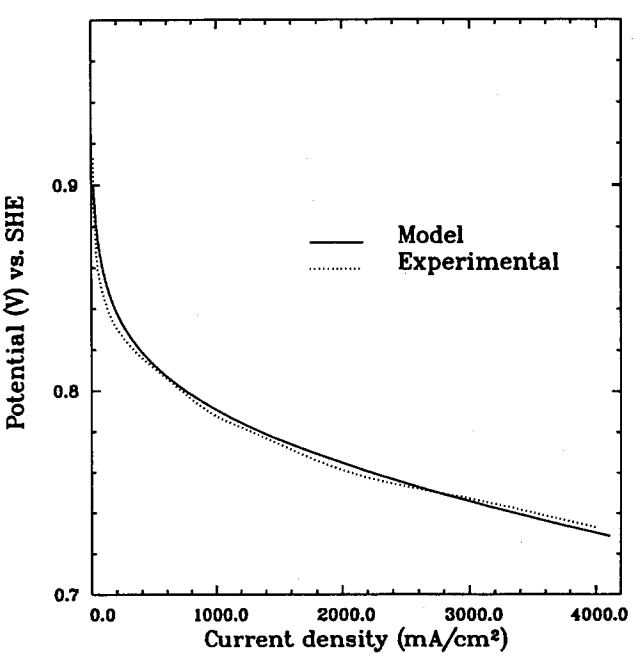

Fig. 6. Model predictions vs. experimental data from 10% TFE sample

Table V. Model parameters used when comparing with 10% TFE data

Temperature (T)	= 298.15 K
Total pressure (P_T)	= 1.703×10^5 N/m^2
Relative humidity (h_r)	= 85.0%
Binary diffusion coefficient of O_2 in H_2O ($D^o_{O_2,H_2O}$)	= 2.82×10^{-5} m^2/s [Ref. (25)]
Diffusion coefficient of dissolved O_2 (D_{O_2})	= 1.90×10^{-9} m^2/s [Ref. (26)]
Diffusion coefficient of H^+ in water (D_{H^+})	= 9.31×10^{-9} m^2/s [Ref. (16)]
Diffusion coefficient of HSO_4^-	= 1.33×10^{-9} m^2/s [Ref. (16)] in water ($D_{HSO_4^-}$)
Solubility of O_2 in electrolyte ($C^o_{O_2}$)	= 9.74×10^{-6} mol/N m [Ref. (26)]
Porous layer thickness (Z^*_l)	= 2.0×10^{-4} m
Active layer thickness (Z_l)	= 2.0×10^{-5} m
Reference concentration (C_{ref})	= 920 mol/m^3
Reference potential at I_{Er} (E_r)	= 0.90V
Reference current density at E_r (I_{Er})	= 184 A/m^2
Tafel slope (T_s)	= 0.0581 V
Fraction of electrode consisting of agglomerates (E_n)	= 0.50
Agglomerate porosity-tortuosity factor (E_a)	= 0.25
Porous layer porosity-tortuosity factor (E_P)	= 0.25
Active layer porosity-tortuosity factor (E_T)	= 0.25
Agglomerate radius (r_a)	= 2.0×10^{-5} m
Conductivity of the electrode (σ_c)	= 100 Ω^{-1} m^{-1}

able parameters θ_1 and θ_2 had very little effect on the predicted polarization curves. This suggests that the performance of the electrode is virtually independent of the porosities and tortuosities of the porous backing and active layers. Similar results were seen when θ_3 was varied over the range from $\theta_3 = 0.20$ to $\theta_3 = 2.0 \times 10^{-3}$ Ω m; that is, changing the specific conductivity (σ_c) of the active layer had very little effect on the performance of the electrode.

The parameter θ_4 was varied by holding the fraction of the electrode consisting of agglomerates, E_n, constant at a value of 0.5 and the agglomerate porosity/tortuosity factor, E_a, constant at 0.25 while varying the agglomerate radius, r_a. Using a PTFE-carbon black composite porous electrode, Klinedinst (22) determined the agglomerate radius to be on the order of 10^{-6}m. To evaluate the effect of the agglomerate radius on the predicted polarization curves, r_a was varied over a range from 2.0×10^{-5} to 2.0×10^{-7}m. Thus, θ_4 varied from 5.7×10^{-5} to 5.7×10^{-7}m. The same results would be obtained if either E_n or E_a were varied while holding r_a constant over the same range of θ_4. Figure 7 shows the polarization curves for three values of θ_4. The performance increases as θ_4 decreases until a certain point

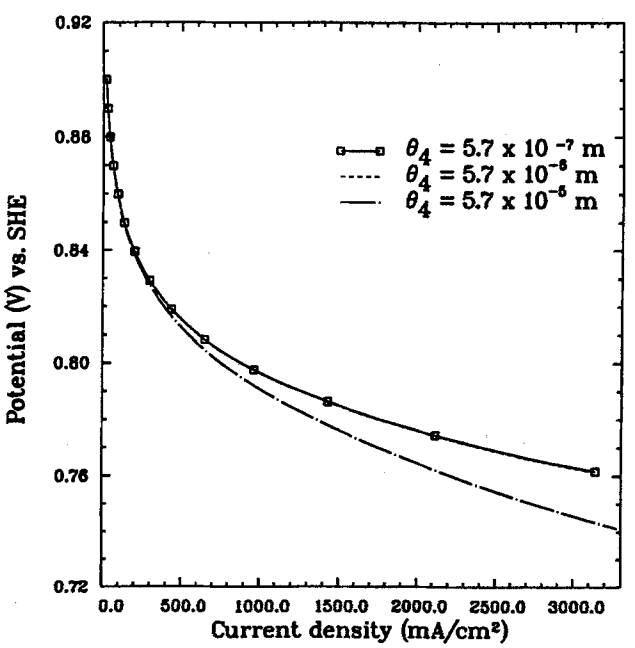

Fig. 7. Effect of θ_4 on performance

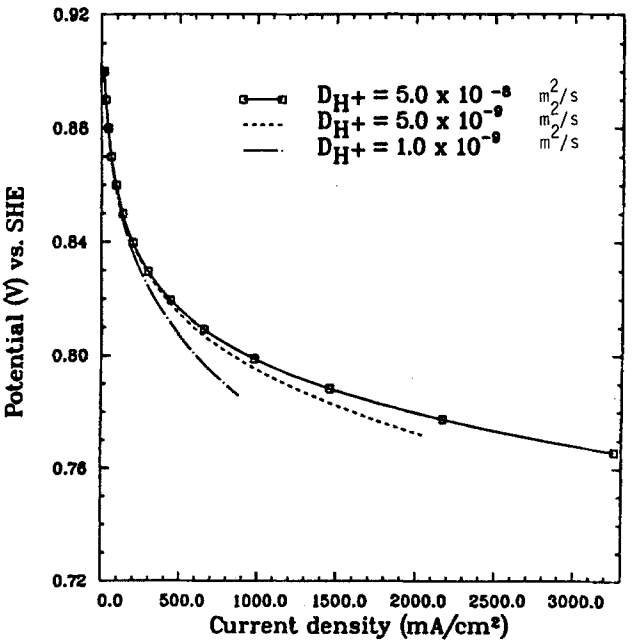

Fig. 8. Effect of D_{H^+} on performance with $r_a = 2.0 \times 10^{-6}$m

is reached after which decreasing θ_4 does not increase the performance any further. As shown in Fig. 7, the polarization curve is shifted upward when θ_4 is decreased from 5.7×10^{-5} to 5.7×10^{-6}m but is the same when θ_4 is decreased further to 5.7×10^{-7}m. This seems reasonable because making the agglomerate radius smaller makes the diffusion path for the dissolved oxygen smaller. However, a certain point is reached when the agglomerate radius is small enough to prevent the diffusion limitations from hindering the electrode performance. Consequently, as the model predictions show, the performance of the electrode increases as the agglomerate radius is decreased until $r_a = 2.0 \times 10^{-6}$m, after which decreasing the agglomerate radius further has no effect on the electrode performance. The value for the agglomerate radius used in comparing the 10% TFE data with the model predictions is 2.0×10^{-5}m (see Fig. 6 and Table V) which corresponds to the value of $\theta_4 = 5.7 \times 10^{-5}$m as shown in Fig. 7. Thus if the agglomerate radius can be made smaller, better performance should result. It may be possible to do this by using smaller platinum particles. If so, this would be consistent with the results in Table III.

To predict the importance of the transport of H^+ ions, r_a was set equal to a small value ($r_a = 2.0 \times 10^{-6}$) and the hydrogen ion diffusion coefficient, D_{H^+}, was varied over the range from 5.0×10^{-8} to 1.9×10^{-9} m^2/s to obtain the predicted polarization curves presented in Fig. 8. This figure shows that limitations associated with the transport of hydrogen ions has a large effect on the performance of the electrode. Therefore, in order to make a better performing electrode, the mechanism for the transport of hydrogen ions to the catalyst site needs to be enhanced. This could be done by adding ionomer to the active layer of the electrode as was first suggested by Schutz (23) and was later shown by Srinivasan *et al.* (24).

Conclusions

A mathematical model for a Teflon®-bonded, platinum black porous electrode has been developed for predicting the performance of a PEM test cell cathode. To gain a better understanding of the limiting processes occurring in the electrode, the transport and reaction of both oxygen and hydrogen ions were included in a model of the electrode. Model predictions agreed well with experimental results that were obtained using a PEM-sulfuric acid test cell. Additional model predictions showed that transport of hydrogen ions to the catalyst site has an effect on the performance of the electrode, whereas gas diffusion has very little effect on the performance of the electrode. Also, according to model predictions, it may be possible to im-

prove the performance of gas-fed electrodes by making agglomerates with small radii.

Manuscript submitted July 14, 1988; revised manuscript received Nov. 29, 1989.

Dow Chemical USA, assisted in meeting the publication costs of this article.

LIST OF SYMBOLS

a	area of electrolyte film per m^3 of electrode (m^2/m^3)
C	total gas concentration (mol/m^3)
C_i	concentration of species i in the agglomerate (mol/m^3)
$C^o_{O_2}$	solubility of oxygen in the electrolyte at a partial pressure of 1 atm (mol/N m)
$C_{O_2}(r_a, Z)$	concentration of oxygen at the film-agglomerate interface (mol/m^3)
D_i	diffusion coefficient of species i (m^2/s)
$D_{i,j}^{eff}$	effective diffusion coefficient of component i in component j (m^2/s)
$D_{i,j}^o$	binary diffusion coefficient of component i in component j (m^2/s)
E	potential difference between the electrode potential and the solution potential (*i.e.*, $E = V - \Phi$) (V)
E_a	porosity/tortuosity factor for the agglomerates (dimensionless)
E_n	fraction of the electrode consisting of agglomerates (dimensionless)
E_p	porosity/tortuosity factor for gas diffusion in porous layer (dimensionless)
E_r	reference potential at I_{Er} (V)
E_{ref}	measured potential at $Z = Z_l$(V)
E_T	porosity/tortuosity factor for gas diffusion in active layer (dimensionless)
$\mathbf{F}$	Faraday constant (96,487 C/mol)
h_r	relative humidity (dimensionless)
I_{act}	activation current density (A/m^2)
I_e	electronic current density in the active layer (A/m^2)
I_{Er}	reference current density at E_r (A/m^2)
K_e	rate constant for the electrochemical reaction of oxygen (s^{-1})
K'_e	rate constant for the electrochemical reaction of oxygen and hydrogen ions ($m^3/mol\ s$)
m	number of components in the gas phase (dimensionless)
M_c	modulus for the active layer (dimensionless)
n	total moles of gas (mol)
N_i	flux of component i (mol/m^2-s)
P_i	partial pressure of component i (N/m^2)
$P^o_{O_2}$	partial pressure of oxygen at $Z^* = 0$ (N/m^2)
$P^*_{H_2O}$	vapor pressure of water (N/m^2)
P_T	total gas pressure (N/m^2)
r_a	radius of agglomerates (m)
R	gas constant (8.3143 N m/K mol)
R'_i	electrochemical rate of reaction at a given point ($mol/m^3\ s$)
T	temperature (K)
T_s	Tafel slope (V/decade)
u_i	mobility of species i in solution ($mol\ cm^2/J\ s$)
v	total gas volume (m^3)
V	potential in the electrode (V)
X_i	mole fraction of species i in the gas phase (dimensionless)
z_i	charge number of species i
Z	position in active layer (m)
Z^*	position in porous layer (m)
Z_l	thickness of active layer (m)
Z^*_l	thickness of porous layer (m)

Greek Letters

δ	thickness of the electrolyte layer (m)
ϵ_c	catalyst effectiveness factor (dimensionless)
Φ	potential in the electrolyte (V)
σ_c	conductivity of the active layer ($\Omega^{-1}\ m^{-1}$)
θ_α	parameter (α = 1-4)

REFERENCES

1. A. J. Appleby and E. B. Yeager, in "Assessment of Research Needs for Advanced Cells," DOE/ER/30060-T1 (Nov. 1985).
2. L. G. Austin, in "Handbook of Fuel Cell Technology," C. Berger, Editor, Prentice Hall, Englewood Cliffs, NJ (1968).
3. L. G. Austin, M. Ariet, R. D. Walker, G. B. Wood, and R. H. Comyn, *Ind. Eng. Chem. Fundam.*, **4,** 321 (1965).
4. F. G. Will, *This Journal,* **110,** 152 (1963).
5. J. Giner and C. Hunter, *ibid.*, **117,** 1124 (1969).
6. R. Darby, *Adv. Energy Convers.*, **5,** 43 (1965).
7. R. E. White, M. A. Nicholson, L. G. Kleine, J. Van Zee, and R. Darby, *This Journal,* **131,** 268 (1984).
8. R. P. Iczkowski and M. B. Cutlip, *ibid.*, **127,** 1433 (1980).
9. M. B. Cutlip, S. C. Yang, and P. Stonehart, in "Electrochemical and Thermal Modeling of Battery, Fuel Cell, and Photoenergy Conversion Systems," J. R. Selman and H. C. Maru, Editors, p. 267, The Electrochemical Society Softbound Proceedings Series, Pennington, NJ (1986).
10. P. N. Ross, *This Journal,* **127,** 2655 (1980).
11. H. J. R. Maget, in "Handbook of Fuel Cell Technology," C. Berger, Editor, p. 455, Prentice Hall, Englewood Cliffs, NJ (1968).
12. J. Redepenning and F. C. Anson, *J. Phys. Chem.*, **91,** 4549 (1987).
13. M. Lopez, B. Kipling, and H. L. Yeager, *Anal. Chem.*, **49,** 629 (1977).
14. R. B. Bird, W. E. Stewart, and E. N. Lightfoot, "Transport Phenomena," John Wiley & Sons, Inc., New York (1960).
15. C. J. Geankoplis, "Mass Transport Phenomena," p. 159, Holt, Rinehart and Winston, Inc., New York (1972).
16. J. S. Newman, "Electrochemical Systems," Prentice-Hall, Inc., Englewood Cliffs, NJ (1973).
17. A. Damjanovic, D. B. Sepa, and M. V. Vojnovic, *Electrochim. Acta,* **24,** 887 (1979).
18. M. B. Cutlip, *ibid.*, **20,** 767 (1975).
19. C. Y. Yuh and J. R. Selman, *This Journal,* **131,** 2062 (1984).
20. B. Carnahan, H. A. Luther, and J. O. Wilkes, "Applied Numerical Methods," John Wiley & Sons, Inc., New York (1969).
21. R. E. White, C. W. Walton, D. J. Wolfe, and K. Plowman, *Chem. Eng. Commun.*, **38,** 229 (1985).
22. K. A. Klinedinst, W. M. Vogel, and P. Stonehart, *J. Mater. Sci.*, **11,** 794 (1976).
23. P. Schutz, M. S. Thesis, Virginia Polytechnic Institute and State University, Blacksburg, VA (1979).
24. S. Srinivasan, E. A. Ticianelli, C. R. Derouin, and A. Redondo, *J. Power Sources,* **22,** 359 (1988).
25. F. A. Schwertz and J. E. Brow, *J. Chem. Phys.*, **19,** 640 (1951).
26. K. E. Gubbins and R. D. Walker, Jr., Abstract 3, p. 7, The Electrochemical Society Extended Abstracts Battery Division, Washington, DC, Oct. 11-15, 1964.